

## Supplementary Information

# A Non-Invasive Approach to the Resistive Switching Physical Model of Ultra-Thin Organic-Inorganic Dielectric-based RRAM

Alba Martinez<sup>1</sup>, Byung Jin Cho<sup>2,\*</sup>, Min Ju Kim<sup>3,\*</sup>

<sup>1</sup> Department of Materials Science Engineering, Korea Advanced Institute of Science and Technology, Daejeon, 34142, Republic of Korea

<sup>2</sup> School of Electrical Engineering, Korea Advanced Institute of Science and Technology, Daejeon, 34142, Republic of Korea

<sup>3</sup> School of Electronics and Electrical Engineering, Dankook University, Gyeonggi-do, 16890, Republic of Korea

\* Corresponding author: Byung Jin Cho, Min Ju Kim

Tel.:

E-mail address: bjcho@kaist.edu, minju9062@dankook.ac.kr

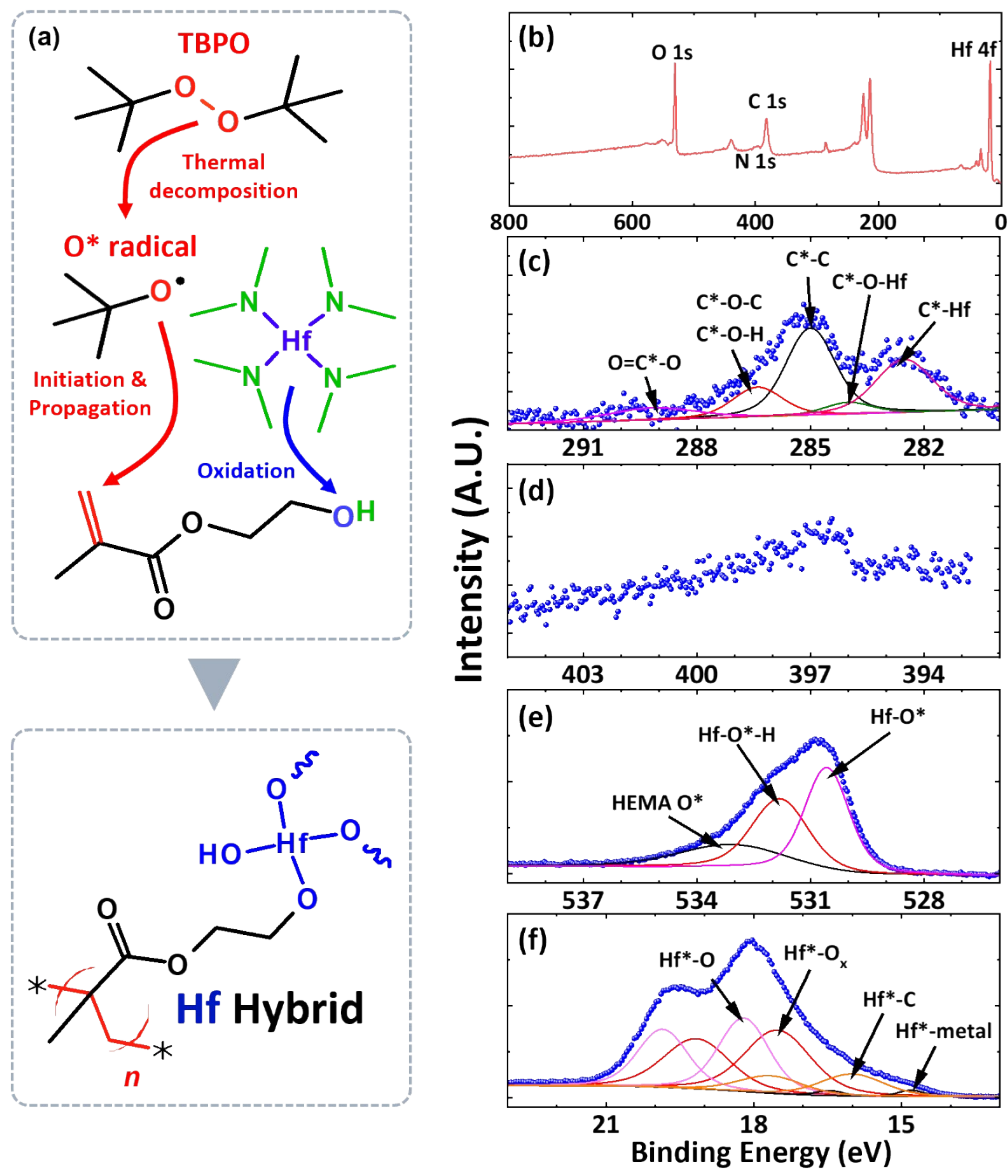


**Figure S1.** (a) Schematic illustration of the organic-inorganic Hf hybrid film synthesis via iCVD process for the H-ReRAM matrix. High-resolution XPS (b) survey, (c) C 1s, (d) N 1s, (e) O 1s, and (f) Hf 4f orbitals spectra of Hf hybrids.

## 1. Characterization of functionalities in the Hf hybrid

In C 1s high-resolution spectra (Figure S1c), the carbon bonding peaks are at the following energy levels: 289.0 (O-C\*=O), 286.5 (C\*-O/C\*-O-H), 285.0 (C\*-C/C\*-C-O), 283.9 (C\*-O-Hf), and 282.5 (C\*-Hf) eV. The presence of a small amount of metallic C\*-Hf bonding suggests its potential role in assisting the filament formation within the hybrid matrix. In the N 1s high-resolution spectra (Figure S1d), a small peak related to nitrogen is observed at 400 eV, indicating the presence of Hf-N\*-C bonding (Hf-N\*-C). The O 1s high-resolution spectra (Figure S1e) show the following peaks corresponding to oxygen bonding: 533.0 (O\* in HEMA matrix), 531.9 (Hf-O\*-H), 530.2 eV (Hf-O\*). The Hf 4f spectra (Figure S1f) further confirm the presence of Hf-OH and Hf-O bonding, in agreement with the FTIR analysis results from Figure 2(b). The Hf-O-H and Hf-O peaks in the Hf 4f spectra align with the observed with -OH peak at 3400 cm<sup>-1</sup>, metal-OH vibration peak around 900 cm<sup>-1</sup>, and metal-O vibration peak around 600 cm<sup>-1</sup> in FTIR spectra.

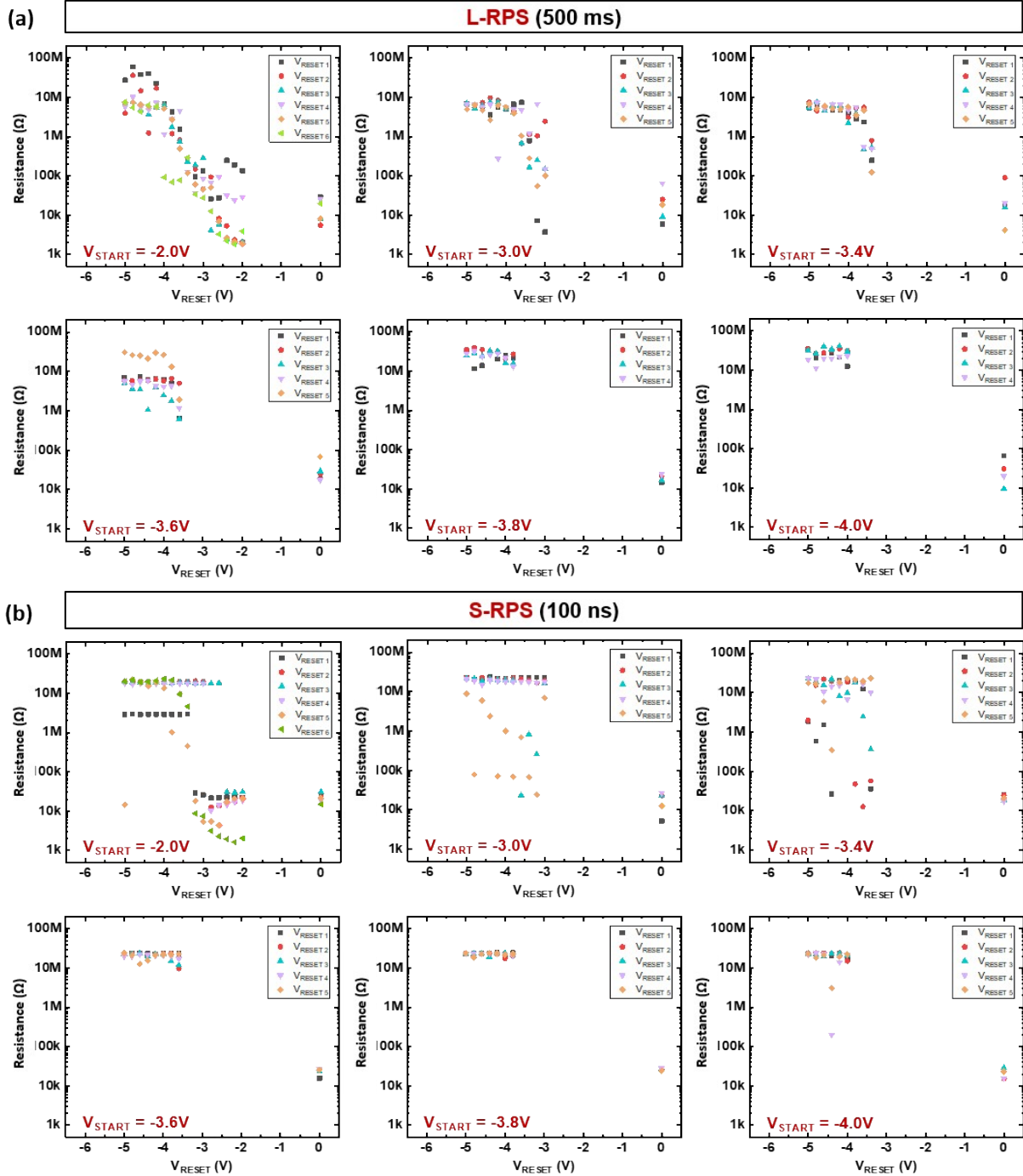


**Figure S2.** RPS measurement of the switching resistance from LRS to HRS at every RPS-step for each  $V_{\text{START}}$  at (a) 500 ms, and (b) 100 ns pulse widths. Each color represents a new switching cycle, where  $V_{\text{RESET}} = 0\text{V}$  is the initial resistance state before applying the reset RPS bias, and every consecutive dot is a new step in the series from the corresponding  $V_{\text{START}}$  to the final  $n^{\text{th}}$  step, or  $V_{\text{END}}$ .

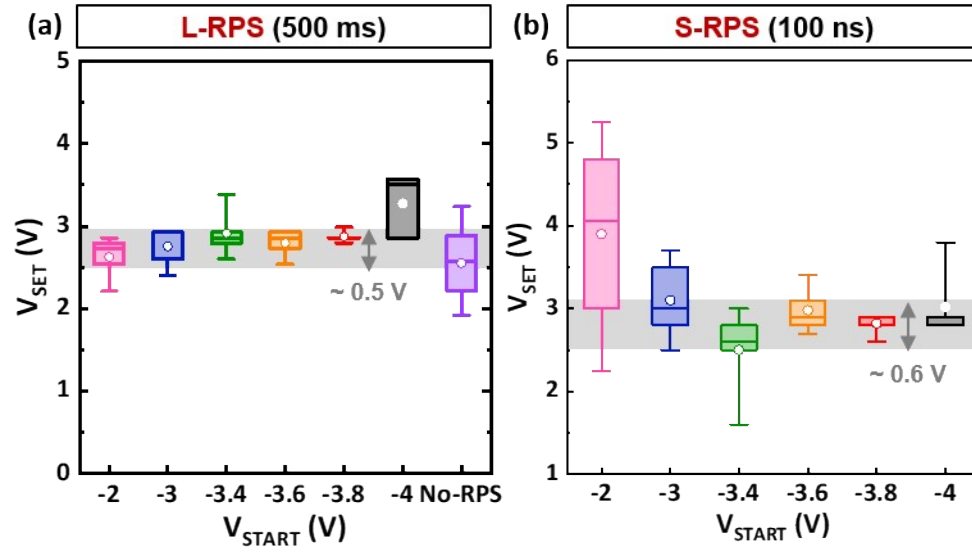


**Figure S3.** Measurement of  $V_{SET}$  after RPS-processed RESET for each  $V_{START}$  at (a) 500 ms (in purple, data referring to the non-RPS-processed case) and (b) 100 ns.

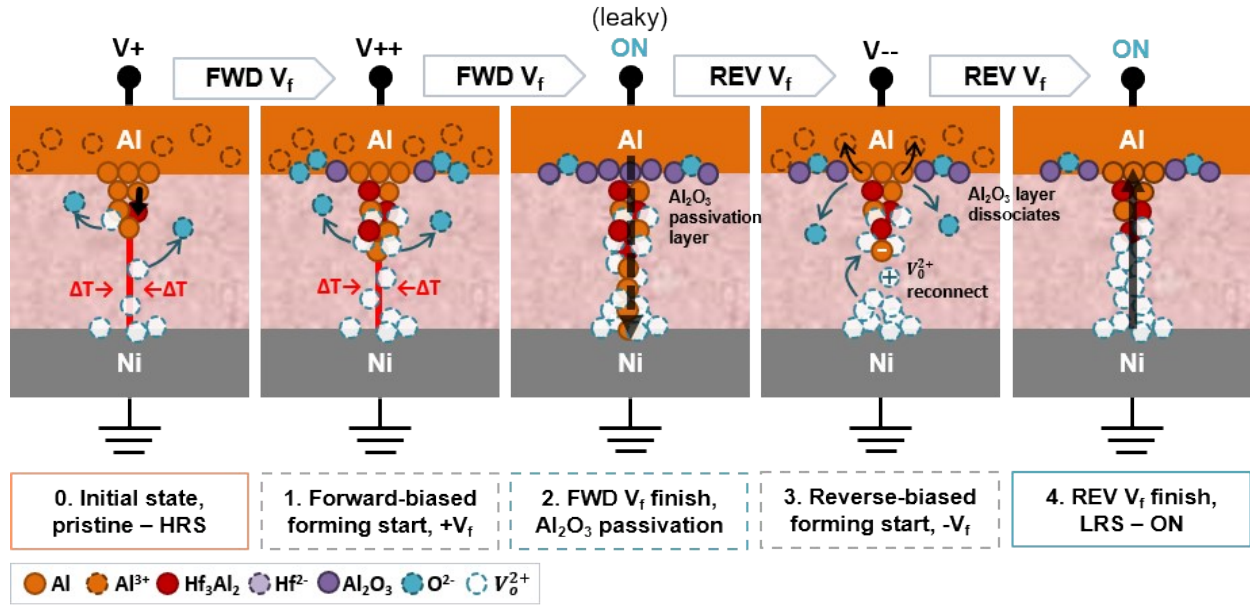


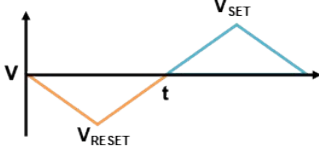
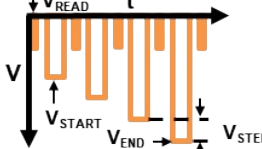
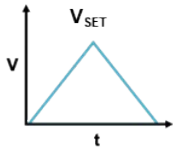
**Figure S4.** Illustration of leaky ON-state filament dynamics in the Hf H-ReRAM devices under a forward-biased (FWD  $V_f$ ) electroforming process, and the reverse bias-induced restoring of the filament (REV  $V_f$ ).

#### 4. Failure mechanism of leaky ON-state CF during forward-biased electroforming.

During the electroforming process in ReRAM devices, a strong forward bias is applied, causing the migration of oxygen ions ( $O^{2-}$ ) in the  $HfO_x$  dielectric towards the Al(TE). At the Al(TE)/Hf-dielectric interface, these  $O^{2-}$  are oxidized into non-lattice oxygen atoms ( $O_2$ ), resulting in an oxygen-rich region (Figure S4, step 0). This region is susceptible to the formation of an  $Al_2O_3$  interlayer, which acts as a passivation layer for the formed conductive filament (CF) (step 1)<sup>1</sup>. The presence of the  $Al_2O_3$  interlayer allows for leaky ON-states to be realized, as electrons tunnel through the oxide passivation layer and into the CF (step 2)<sup>2, 3</sup>. This behavior can be confirmed by applying a reverse-biased forming voltage, which removes the leaky ON-state and reveals well-connected electrodes. During the reverse bias, the  $Al_2O_3$  interlayer dissociates into Al ions ( $Al^{3+}$ ) and  $O^{2-}$ . The  $Al^{3+}$  diffuse into the negatively charged Al(TE), while the  $O^{2-}$  diffuse back into the dielectric (step 3). Due to the heated region of the CF, Soret diffusion

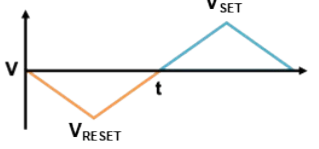
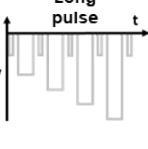
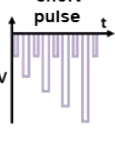
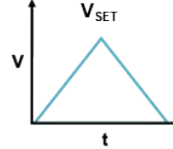
causes the  $O^{2-}$  to prefer to recombine with the bulk oxygen vacancies ( $V_o^{2+}$ ). As a result, the remaining  $V_o^{2+}$  at the CF drift towards the virtually negative Al-CF tip to fully connect the filament and achieve a complete ON-state (step 4).

Table S1. Detailed resistive switching process steps for the (a) amplitude, (b) pulse width and (c) temperature modulated RPS tests.

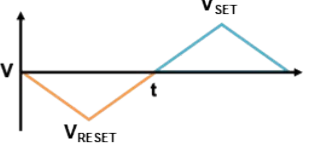


(a)	STABILIZATION		RPS-RESET				SET
	$V_{\text{RESET}}$	$V_{\text{SET}}$	$V_{\text{START } i}$	$V_{\text{STEP}}$	$V_{\text{END}}$	$V_{\text{READ}}$	$V_{\text{SET}}$
Operating voltage (V)	-5.0	6.0	$i$	-0.2	-5.0	-1.0	6.0
Pulse scheme							
Pulse width (s)	>0.5	>0.5	0.5				>0.5
Current Compliance ( $\mu\text{A}$ )	N/A	100	N/A				100

Where  $i = -2.0, -3.0, -3.4, -3.6, -3.8, -4.0$

(b)	STABILIZATION		RPS-RESET				SET
	$V_{\text{RESET}}$	$V_{\text{SET}}$	$V_{\text{START}}$	$V_{\text{STEP}}$	$V_{\text{END}}$	$V_{\text{READ}}$	$V_{\text{SET}}$
Operating voltage (V)	-5.0	6.0	-3.6	-0.2	-4.2	-1.0	6.0
Pulse scheme							
Pulse width (s)	>0.5	>0.5	0.5	$10^{-4}$	$10^{-7}$		>0.5
Current Compliance ( $\mu\text{A}$ )	N/A	100	N/A				100

(c)	STABILIZATION		RPS-RESET				SET
	$V_{\text{RESET}}$	$V_{\text{SET}}$	$V_{\text{START}}$	$V_{\text{STEP}}$	$V_{\text{END}}$	$V_{\text{READ}}$	$V_{\text{SET}}$
Operating voltage (V)	-5.0	6.0	-3.4	-0.2	N/A	-1.0	6.0
Pulse scheme							
Process T (K)	room T	room T	300	330	360	390	
Pulse width (s)	>0.5	>0.5	$10^{-7}$				>0.5
Current Compliance ( $\mu\text{A}$ )	N/A	100	N/A				100



## Reference

1. Yuan, F.-Y.; Deng, N.; Shih, C.-C.; Tseng, Y.-T.; Chang, T.-C.; Chang, K.-C.; Wang, M.-H.; Chen, W.-C.; Zheng, H.-X.; Wu, H., Conduction mechanism and improved endurance in HfO<sub>2</sub>-based RRAM with nitridation treatment. *Nanoscale research letters* **2017**, *12* (1), 574.
2. Yu, S.; Wu, Y.; Wong, H.-S. P., Investigating the switching dynamics and multilevel capability of bipolar metal oxide resistive switching memory. *Applied Physics Letters* **2011**, *98* (10), 103514.
3. Chang, K.-C.; Chang, T.-C.; Tsai, T.-M.; Zhang, R.; Hung, Y.-C.; Syu, Y.-E.; Chang, Y.-F.; Chen, M.-C.; Chu, T.-J.; Chen, H.-L., Physical and chemical mechanisms in oxide-based resistance random access memory. *Nanoscale research letters* **2015**, *10* (1), 1-27.